Flutter of Circulation Control Wings

David J. Haas*
David Taylor Research Center, Bethesda, Maryland
and
Inderjit Chopra†
University of Maryland, College Park, Maryland

The flutter instability of a high aspect ratio circulation control (CC) wing is examined using a lumped-parameter approach in conjunction with a modified unsteady aerodynamic strip analysis method. A low-speed flutter instability unique to wings employing circulation control blowing is identified. This phenomenon, termed "CC flutter," is a single-degree-of-freedom bending mode instability. The origin of the instability is the negative lift curve slope that occurs at combinations of moderate angle of attack and high blowing level. The effects of several design parameters on CC flutter are presented, including blowing level, torsion stiffness, bending stiffness, wing sweep angle, and spanwise blowing distribution. Unlike classical flutter, CC flutter depends on wing bending stiffness rather than the ratio of torsion-to-bending stiffness. A relative reduction of outboard blowing is shown to be beneficial for aeroelastic stability of circulation control wings.

Nomenclature

a = nondimensional distance from midchord to elastic axis, positive rearward, fraction of b
a_c = nondimensional distance from midchord to aerodynamic center, positive rearward, fraction of b
b = semichord
$C(k)$ = Theodorsen circulation function
C_{ℓ_α} = lift curve slope
C_μ = blowing momentum coefficient
c = chord, normal to wing leading edge
EI_0 = bending stiffness of baseline wing
$\{F\}$ = aerodynamic force vector
g = structural damping factor
h = bending displacement
$[K]$ = structural stiffness matrix
k = reduced frequency, $k = \omega b/V_n$
L = lift per unit span
$[M]$ = mass matrix
M_α = aerodynamic moment about elastic axis per unit span
$\dot{m}$ = mass flow rate through slot
q = dynamic pressure based on V_n
V = freestream velocity
V_j = calculated jet velocity
V_n = velocity in chordwise direction
x = coordinate in chordwise direction
y = coordinate in spanwise direction
α = local aerodynamic angle of attack in chordwise direction
ζ = damping ratio
θ = torsional displacement
ι = $\sqrt{(-1)}$
λ = system eigenvalue
Λ = wing sweep angle, positive aft
ρ = air density at sea level
σ = bending slope, $\partial h/\partial y$
τ = torsion slope, $\partial\theta/\partial y$
$[\Upsilon]$ = complex matrix of aerodynamic influence coefficients
$[\Phi]$ = matrix of free vibration mode shapes
ω = frequency of vibration
ω_β = first bending frequency
ω_θ = first torsion frequency
$1B$ = first bending mode
$2B$ = second bending mode
$1T$ = first torsion mode
$(\dot{})$ = derivative with respect to time, $\partial(\ )/\partial t$

Received April 17, 1988; presented as Paper 88-2345 at the AIAA ASME/ASCE/AHS 29th Structures, Structural Dynamics and Materials Conference, Williamsburg, VA, April 18–20 1988; revision received July 15, 1988. This paper is declared a work of the U.S. Government and is not subject to copyright protection in the United States.

*Aerospace Engineer, Aviation Department. Member AIAA.
†Professor, Department of Aerospace Engineering. Associate Fellow AIAA.

Introduction

EXPERIMENTATION with circulation control (CC) airfoils as a means of lift augmentation has taken place since the 1950's.[1] Although the first experiments involved circular cylinders, a modern CC airfoil is typically of quasielliptical shape. A small amount of camber is usually added to increase aerodynamic efficiency (see Fig. 1). For a CC airfoil, lift is augmented and controlled by blowing a thin sheet of air through a slot near a rounded trailing edge. Due to the Coanda effect, this sheet of air remains attached and relocates the stagnation point farther below the airfoil. At maximum blowing levels, the lift coefficient of a CC airfoil can be several times greater than that of a conventional airfoil. In addition to lift augmentation, another advantage of circulation control is the capability to easily control lift independent of angle of attack.

In the past, both rotary-wing and fixed-wing aircraft have been tested with CC airfoils. Also, circulation control was used successfully on a helicopter tail boom in place of a conventional tail rotor as a means of reacting main rotor torque and providing directional control.[2] Perhaps the most exciting application of CC airfoils is the stoppable rotor aircraft concept. In the rotary-wing mode, circulation control is used to control cyclic and collective lift; in the fixed-wing or "X-wing" mode of flight, differential blowing can be used to provide lateral and longitudinal control.

To fully incorporate the use of CC airfoils into modern aircraft design, an understanding of the basic aeroelastic behavior of these airfoils is necessary. Much of the research

and experimentation to date has focused on the basic performance of CC airfoils, with only limited research on the aeroelastic instabilities associated with CC airfoils. Chopra[3] examined the aeroelastic stability of CC rotors and found appreciable differences in the stability results as compared to conventional rotors. Haas and Chopra[4] analytically examined the static aeroelastic characteristics of CC wings and showed these characteristics to be substantially different from those of conventional wings. The results of this study[4] indicated that for an accurate assessment of divergence and reversal conditions of CC wings, the nonlinear airfoil characteristics should be included.

Wind-tunnel testing of CC wings has also been very limited. Wilkerson[5] conducted a wind-tunnel test on an isolated CC wing supported at the root by soft springs and observed low-speed instabilities that appeared to be unique to CC airfoils. Recently, a wind-tunnel test involving CC wings was conducted at United Technologies Research Center. In this test, a scaled model of a stoppable rotor aircraft was evaluated in the X-Wing mode. A flutter instability was observed at low speed for some combinations of angle of attack and blowing level. This instability was typically a limit cycle oscillation of the two forward-step wings.

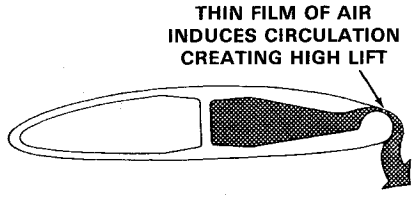

Fig. 1 Typical circulation control airfoil.

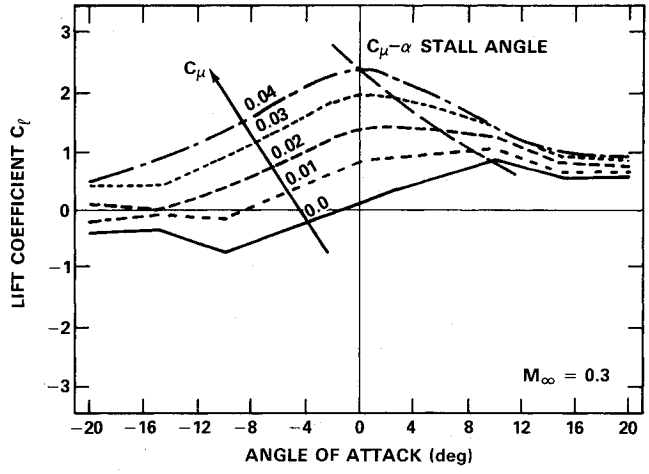

a) Section lift coefficient

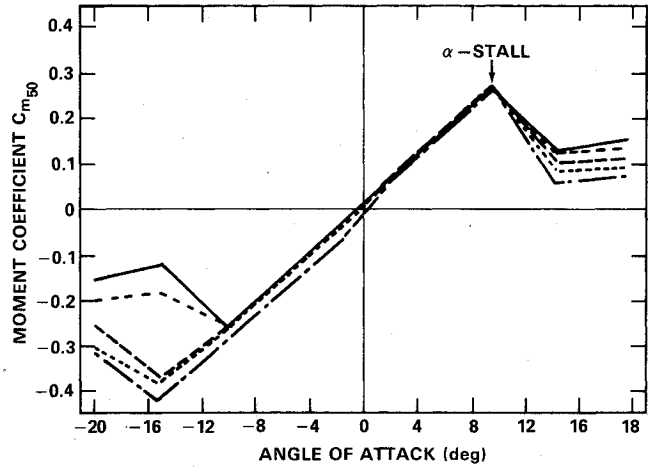

b) Section moment coefficient

Fig. 2 Lift and moment data for typical CC airfoil.

The objective of the present study is to examine the flutter instability of CC wings. Unfortunately, no unsteady aerodynamic data are available for CC airfoils; however, recent analytical investigations[6] suggest that the Theodorsen unsteady aerodynamic approximation appears to be applicable to CC airfoils if the reduced frequency is moderate to low. In order to include static CC airfoil characteristics in the flutter analysis, a computer program based on the modified strip analysis method has been developed.[7] Yates[7] has shown that this method yields good flutter results for conventional wings over a broad range of Mach number, wing taper ratio and wing sweep angle. The modified strip analysis uses linear, Theodorsen-type, unsteady aerodynamics and allows for the incorporation of static airfoil lift and moment data (which can be nonlinear with angle of attack, Mach number and blowing level). Because of its easy implementation, the modified strip method is a very useful tool for gaining insight into new phenomena and, therefore, is chosen for the present investigation.

A large data base of CC airfoil performance data exists at the David Taylor Research Center (DTRC). This data base contains lift and moment coefficients at various levels of blowing over a wide range of angle of attack and Mach number for a given airfoil thickness-to-chord ratio and slot location. These data are used directly in the analysis to calculate flutter speed under different conditions of blowing level and mean angle of attack.

The V-g method of flutter analysis[8] is used to calculate flutter boundaries. The wing is modeled structurally as an elastic beam, and a lumped parameter formulation is adopted to obtain structural, inertial, and aerodynamic influence coefficients. Using the V-g flutter analysis method, an instability unique to CC wings is identified. The effect of several design parameters on flutter stability is investigated, and some qualitative trends are established.

Circulation Control Aerodynamics

The lift on a CC airfoil can be divided into two components: the lift due to angle of attack and the lift due to blowing. The blowing level is characterized by a blowing momentum coefficient C_μ defined as

$$C_\mu = \dot{m}V_j/qc$$

Blowing level is controlled by pneumatic valving that varies both the mass flow and pressure in the duct. Because C_μ is nondimensionalized by q, large values of C_μ typically can be generated only at relatively low speeds. In the present study, it is assumed that the blowing level C_μ is held constant with forward speed by a control system that increases the jet momentum ($\dot{m}V_j$) as required.

Each of the components of lift has an aerodynamic center associated with it. The aerodynamic center for angle-of-attack lift is located near the quarter-chord (similar to a conventional airfoil); the aerodynamic center for lift due to blowing is located near the half-chord. In Figs. 2a and 2b, the lift and moment at the half-chord for a typical CC airfoil are plotted with varying angle of attack for several values of C_μ. (Generally, circulation control data are resolved at the half-chord because the aerodynamic center associated with blowing is located near this position.)

The data in Fig. 2 show two types of stall phenomena. The first is analogous to classical stall in that it is associated with flow separation at high angles of attack. This "α-stall" is recognized by a change in sign of the slope of the half-chord

pitching moment curve. This type of stall does not depend on the blowing level, and for the present airfoil, α-stall occurs at about 10 deg.

The second type of stall, "C_μ-α stall," occurs when blowing is present. The C_μ-α stall is characterized by a change in sign of the lift curve slope with respect to angle of attack and occurs before α-stall. The mechanism for C_μ-α stall is a decrease in boundary-layer control effectiveness due to a thickening of the airfoil boundary layer as angle of attack is increased. When this occurs, the component of lift produced by blowing decreases rapidly as α is increased such that there is a net decline in total lift and, hence, stall. There is little or no change in the pitching moment about half-chord. The angle of C_μ-α stall depends on the blowing level and typically (depending on airfoil thickness ratio and C_μ level) decreases as blowing is increased. Generally, the flow remains attached to the airfoil up to the point of α-stall, even though the lift behaves as though the airfoil were stalled beyond the angle of C_μ-α stall (i.e., decreasing lift with increasing α). Because the flow remains attached, the use of Theodorsen's unsteady aerodynamic approximation is assumed to be valid in this C_μ-α stall region.

Due to the gradual stall characteristics of CC airfoils, it is possible for these airfoils to operate beyond the C_μ-α stall angle of attack. A more detailed description of CC aerodynamics is found in Refs. 9 and 10.

Flutter Analysis Technique

The V-g method of flutter analysis[8] is used to calculate the flutter stability boundary of a CC wing with an aspect ratio of 10. The wing is modeled as an elastic beam clamped at the root undergoing bending and torsion deformation (Fig. 3). Because of the complexity of the problem and the lack of unsteady circulation control data, the modified strip analysis method[7] is used to obtain the unsteady aerodynamic forces. With this modified strip method, static experimental CC airfoil lift and moment data can be included directly in the flutter calculation. Three-dimensional aerodynamic effects have been ignored, so the local aerodynamic angle of attack is taken to be the wing incidence angle.

The equations of motion are derived using a lumped-parameter approach. In matrix notation, the equations of motion can be written as

$$[M]\{\ddot{q}\} + [K]\{q\} = \{F\} \tag{1}$$

where $[M]$ is the structural mass matrix that contains the mass and moment of inertia of each chordwise strip along the span of the wing, and $\{q\}$ is the vector of vertical displacements h and torsional rotations θ for each strip.

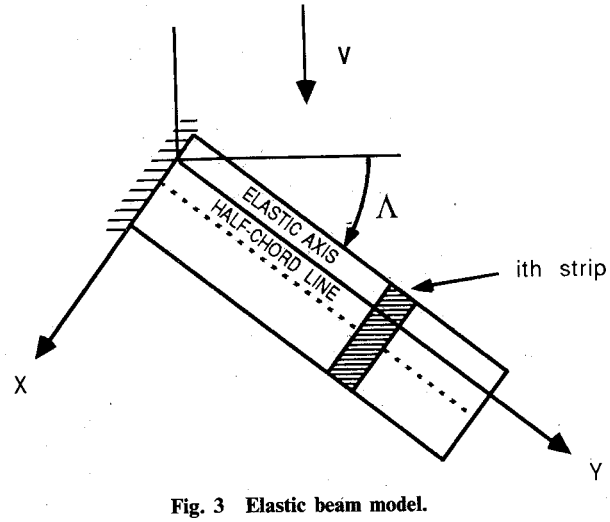

Fig. 3 Elastic beam model.

Unsteady lift L and moment M_α about the elastic axis per unit span, taken from the modified strip analysis,[7] can be written as

$$\begin{aligned} L &= \pi\rho b^2[\ddot{h} + V_n\ddot{\theta} + V_n\dot{\sigma}\tan\Lambda - ba(\ddot{\theta} + V_n\dot{\tau}\tan\Lambda)] \\ &\quad + C_{\ell_\alpha}\rho V_n b C(k) Q \\ M_\alpha &= -\pi\rho b^4(1/8 + a^2)(\ddot{\theta} + V_n\dot{\tau}\tan\Lambda) \\ &\quad + \pi\rho b^2 V_n(\dot{h} + V_n\sigma\tan\Lambda) \\ &\quad + \pi\rho b^3 a(\dot{h} + V_n\dot{\sigma}\tan\Lambda) + \pi\rho b^2 V_n^2(\theta - ab\tau\tan\Lambda) \\ &\quad - 2\pi\rho V_n b^2[1/2 - (a - a_c)C(k)C_{\ell_\alpha}/2\pi]Q \end{aligned} \tag{2}$$

where

$$Q = \dot{h} + V_n\theta + V_n\sigma\tan\Lambda + b(C_{\ell_\alpha}/2\pi + a_c - a)(\dot{\theta} + V_n\tau\tan\Lambda)$$

This two-dimensional aerodynamic representation assumes harmonic motion of the airfoil.

The forces for each of the strips can be assembled into a total force vector $\{F\}$ for the wing. In matrix form, the force vector can be expressed as

$$\{F\} = \pi\rho\omega^2[\Upsilon]\{q\}e^{\imath\omega t} \tag{3}$$

Assuming a solution of the form

$$\{q(y,t)\} = \{q(y)\}e^{\imath\omega t} \tag{4}$$

and substituting Eq. (3) into Eq. (1) yields

$$(-\omega^2[M] + [K])\{q\}e^{\imath\omega t} = \pi\rho^2\omega^2[\Upsilon]\{q\}e^{\imath\omega t} \tag{5}$$

For the V-g method, structural damping is included by multiplying the structural stiffness matrix by $(1 + \imath g)$, where g is typically twice ζ. Introducing structural damping and rearranging terms, Eq. (5) becomes

$$(\pi\rho[\Upsilon] + [M])\{q\} = (1 + \imath g)/(\omega^2)[K]\{q\} \tag{6}$$

Equation (6) is reduced to modal space in the form of normal mode equations by premultiplying and postmultiplying by the matrix $[\Phi]$, which contains the free vibration mode shapes. For flutter analysis, only a few selected modes are used to reduce the number of equations. This results in a complex eigenvalue problem of the form

$$[A]\{q\} = \lambda[B]\{q\} \tag{7}$$

where

$$[A] = [\Phi^t](\pi\rho[\Upsilon] + [M])[\Phi]$$

$$[B] = [\Phi^t][K][\Phi]$$

$$\lambda = (1 + \imath g)/(\omega^2)$$

The solution procedure begins by assuming a large value of k (low velocity), calculating $[\Upsilon]$, and solving Eq. (7) for λ. For each mode g, V, and ω can then be determined from

$$\omega^2 = 1/\text{Real}(\lambda)$$

$$g = \omega^2\,\text{Imag}(\lambda)$$

$$V = \omega b/(k\cos\Lambda)$$

This process is repeated for higher speeds (i.e., lower values of k) so that a plot of damping vs velocity can be compiled.

Instability occurs at the speed where the calculated damping factor g just equals the amount of structural damping available within the structure. At this condition, the total damping is equal to zero, which marks the onset of instability. For zero structural damping, a positive value of g denotes an unstable condition. In the examples presented, g for the wing is assumed to equal 0.05 (damping ratio $\zeta = 2.5\%$), and the first five vibration modes (three bending and two torsion) are included in the analysis.

Results and Discussion

An aeroelastic analysis is conducted on a uniform CC wing with properties representative of a stoppable rotor design with high aspect ratio blades. The wing has a 17% thick, single-slot, quasielliptical airfoil with blowing at the trailing edge. The elastic axis and center of gravity are located at the half-chord position, and the ratio of torsion-to-bending frequency is 9.7. These properties are atypical for a conventional high aspect ratio wing, where the ratio of torsion-to-bending frequency would be much much lower. Table 1 lists the properties for the baseline configuration. Low-speed ($M_\infty = 0.3$) aerodynamic CC airfoil data were used for the flutter analysis, because these data correspond approximately to the speeds at which CC flutter typically occurs.

Figure 4 shows the variation in modal frequencies and damping with velocity for an unswept wing at $\alpha = 4$ deg with no blowing. Both the static divergence instability (when both damping and frequency approach zero) and flutter (when damping approaches zero) occur at nearly the same speed. These instabilities occur at a very high speed where the analysis is not accurate due to compressibility effects. The instability is attributed to the large offset of the aerodynamic center (located approximately at the quarter-chord) from the elastic axis (located at the half-chord), which causes a sharp reduction in torsional stiffness at high speeds. For the expected maximum design speeds of stopped rotor aircraft, approximatley 800 ft/s, the unblown wing is stable from flutter if blowing is not introduced. Below α-stall, the flutter speed of an unblown wing is not dependent on angle of attack.

The effect of blowing on aeroelastic stability is demonstrated with the unswept wing at $\alpha = -4$ deg in Fig. 5. Frequency and damping are shown as a function of velocity with a blowing coefficient of 0.04, representing a high of level blowing at $M_\infty = 0.3$. Because CC wings have the capability to produce large lift coefficients, they can operate efficiently at negative angles of attack. The results presented in Fig. 5 show that even this high level of blowing does not significantly alter the aeroelastic stability of the wing at $\alpha = -4$ deg.

The effect of blowing at $\alpha = 4$ deg for the unswept wing is presented in Fig. 6. The variation of damping with velocity is shown with the blowing coefficient set of 0.02 (moderate blowing) and 0.04 (high blowing), respectively. Comparing Fig. 6 with Fig. 4b, it is evident that the damping changes significantly when blowing is added at $\alpha = 4$ deg. With blowing, the first bending mode becomes unstable with increasing airspeed—quite opposite to that of an unblown wing. The variation of modal frequencies with airspeed, however, is not significantly altered when blowing is added and would be similar to that in Fig. 4a.

To further illustrate the effect of blowing, flutter speed vs blowing level for the wing at $\alpha = -4$ and $+4$ deg is shown in Fig. 7. For convenience, the results are normalized by the flutter speed of the unblown wing at $\alpha = 4$ deg. At $\alpha = -4$ deg, blowing level has little effect on flutter. At $\alpha = 4$ deg, however, blowing has a strong destabilizing effect on flutter stability. These results can be understood by examining the airfoil lift characteristics shown in Fig. 2a.

In Fig. 2a, at $\alpha = -4$ deg, the lift curve slope is positive regardless of blowing level, and the wing flutters (or diverges) at high speed in a classical sense. At $\alpha = 4$ deg, the lift curve slope changes from positive to negative as blowing level is increased from 0 to 0.04. When the lift curve slope changes in sign, the aerodynamic damping in the bending mode becomes negative and the wing becomes unstable. This low-speed bending mode instability is attributed to the unique C_μ-α stall characteristics of CC airfoils and is termed "CC flutter." At a moderate blowing level ($C_\mu = 0.02$), only a small amount of structural damping ($g = 0.052$) is required to stabilize the wing at 500 ft/s, whereas at a high blowing level ($C_\mu = 0.04$), a structural damping factor of $g = 0.23$ is necessary to ensure stability for the same speed. The relatively gradual rise in the $1B$ curves in Figs. 6a and 6b indicates that the CC flutter speed has a high degree of sensitivity to the level of damping present in the structure.

Although CC flutter occurs only at angles of attack above the C_μ-α stall angle, the phenomenon should not be confused

Table 1 Properties of baseline configuration

Aspect ratio	10
ω_β	158 rad/s
ω_θ	1533 rad/s
Mass ratio	94.3
Center of gravity	half-chord
Elastic axis	half-chord
Airfoil	17%, quasielliptic
Slot location	$0.97c$
Slot height-to-chord ratio	0.0015

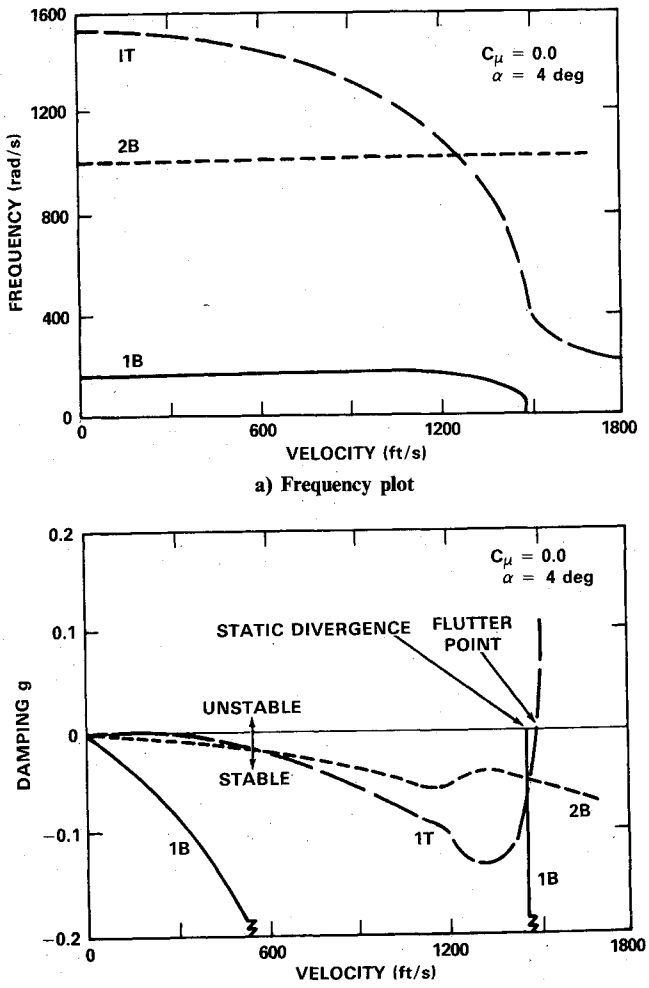

Fig. 4 Unswept wing with no blowing.

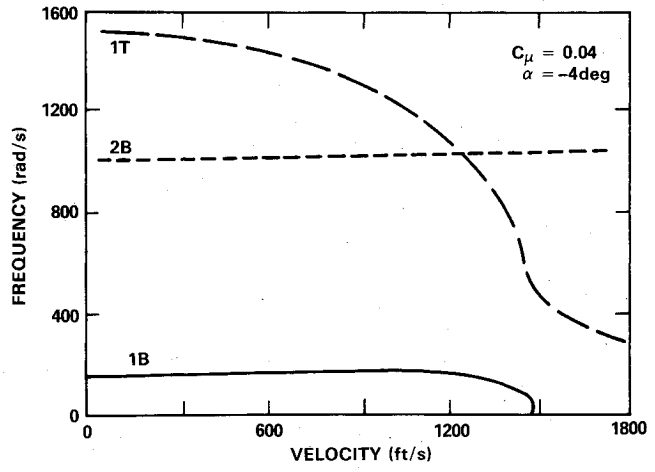

a) Frequency plot

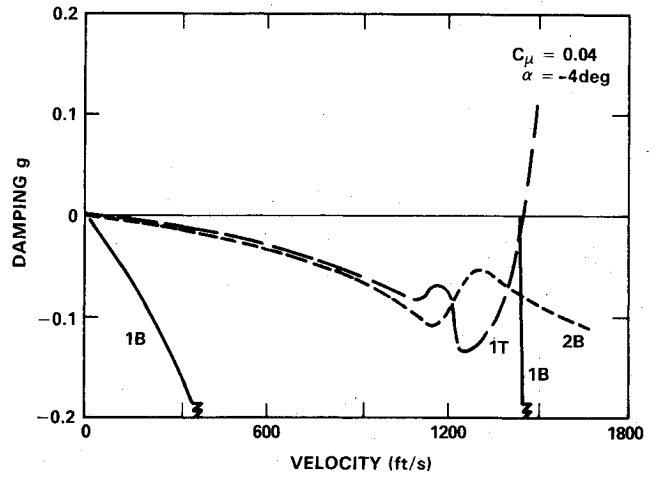

b) Damping plot

Fig. 5 Unswept wing with high blowing.

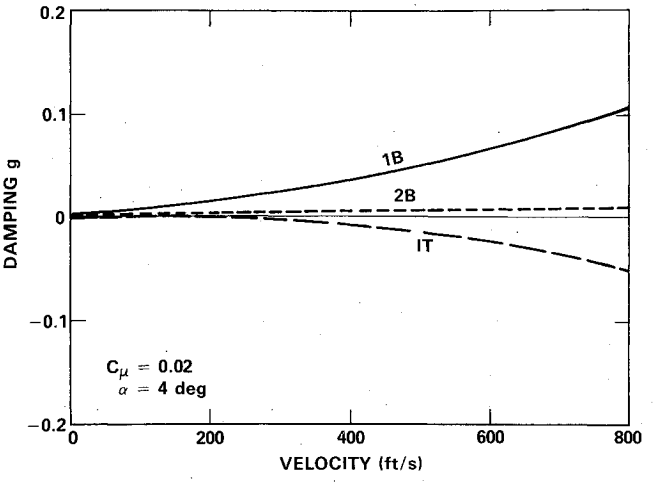

a) Moderate blowing ($C_\mu = 0.02$)

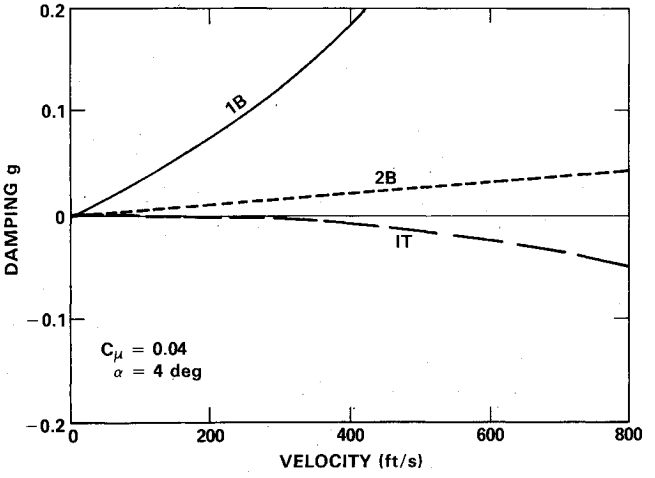

b) High blowing ($C_\mu = 0.04$)

Fig. 6 Unswept wing with moderate and high blowing.

with classical stall flutter. Classic stall flutter involves the hysteresis effect of a conventional airfoil oscillating near the α-stall angle of attack. This hysteresis effect is due to unsteady flow separation and is called dynamic stall. In constrast, the flow on a CC airfoil remains essentially attached up to the α-stall angle, even though the lift coefficient begins to reduce beyond the C_μ-α stall angle. This observation also lends support to the use of the Theodorsen aerodynamic approximation for analysis of CC flutter because the flow is still attached.

As expected, the flutter of the unblown wing at 4 deg occurs due to the coalescence of the bending and torsion modes. When either mode is removed from the analysis, flutter does not take place. With the inclusion of blowing, the instability becomes an uncoupled bending-mode instability. If the first bending mode is removed from the analysis, the wing does not flutter. However, if the first torsion mode is removed, flutter will still take place. This indicates that the flutter associated with the blown wing is a single-degree-of-freedom flutter instability of the bending mode. There is no significant coupling with the torsion mode in this instability.

The effect of wing bending stiffness on CC flutter is shown in Fig. 8 for the unswept wing at $\alpha = 4$ deg and $C_\mu = 0.04$. Three cases are considered: the baseline case, a bending stiffness of 0.6 of the baseline, and a bending stiffness of 2.5 times that of the baseline value. Flutter speeds are normalized by the flutter speed of the baseline wing. The results show that a reduction in bending stiffness is destabilizing, and an increase in bending stiffness is stabilizing to CC flutter. Note

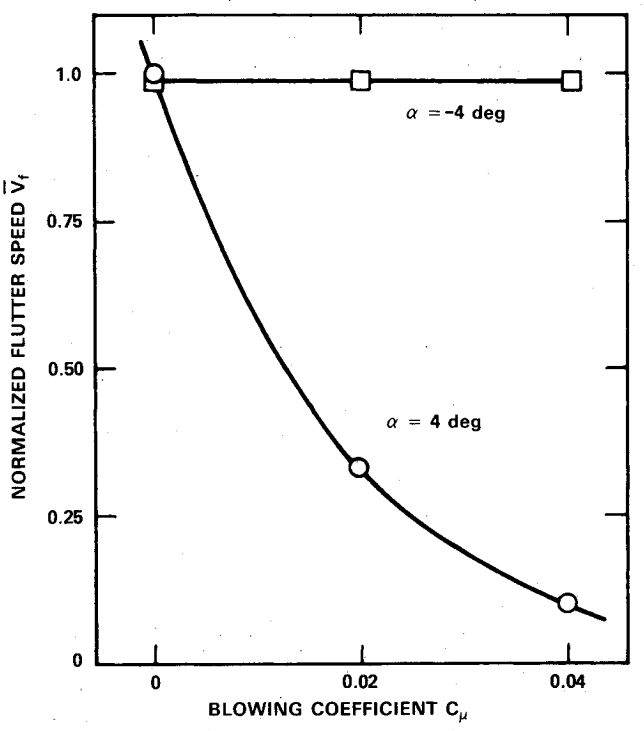

Fig. 7 Variation of normalized flutter speed with blowing coefficient.

Table 2 Flutter results for baseline wing with two aerodynamic models

Aerodynamic model	Classical flutter speed, $\alpha = 4$ deg, $C_\mu = 0$	CC flutter speed, $\alpha = 4$ deg, $C_\mu = 0.04$
Unsteady	1495 ft/s ($k = 0.07$)	140 ft/s ($k = 0.27$)
Quasisteady $C(k) = 1.0$	1236 ft/s ($k = 0.17$)	96 ft/s ($k = 0.40$)

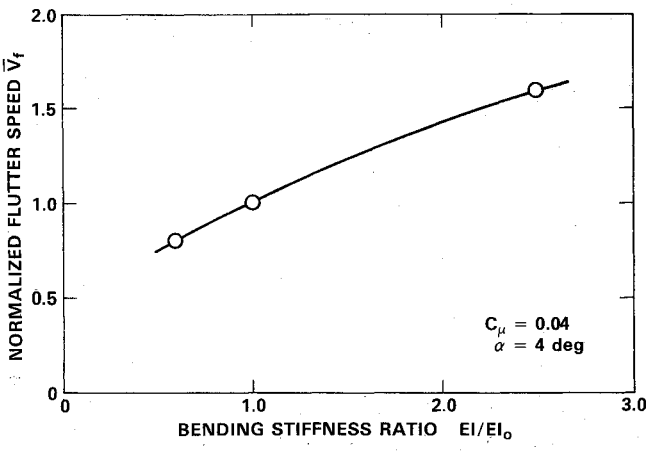

Fig. 8 Effect of bending stiffness on CC flutter.

that relatively large changes in bending stiffness are required to produce appreciable changes in CC flutter speed.

Torsional stiffness GJ for the unswept wing was reduced to 2% of the baseline value. This reduction had a significant effect on the static divergence but only a negligible effect on the CC flutter instability. The elastic axis location was also varied for the baseline wing from $0.1c$ forward to $0.1c$ aft of the half-chord position. No appreciable changes in the CC flutter instability boundary occurred. However, the damping in the torsion mode was appreciably reduced as the elastic axis was moved aft of the half-chord. These results further confirm that CC flutter is a single-degree-of-freedom bending mode instability and is insensitive to changes in the torsion mode or the elastic axis location. Furthermore, unlike classical flutter, CC flutter is a function of the bending frequency rather than the ratio of torsion-to-bending frequencies.

To determine the role of unsteady aerodynamics in this phenomenon, stability calculations for the baseline wing were repeated using quasisteady aerodynamics [Theodorsen function $C(k)$ set equal to one; see Table 2]. With the quasisteady approximation, the CC instability boundary is reduced because of the increase in magnitude of the aerodynamic forces. For the unblown wing, the classical flutter speed is also reduced due to the overall increase in aerodynamic moment in the torsion mode. Note that the reduced frequency for CC flutter is higher than that for classical flutter but is still within the moderate-to-low range.

The effect of wing sweep on CC flutter is examined in Fig. 9 for the baseline wing at $\alpha = 4$ deg at high blowing. Damping in the first bending mode (the least stable mode) is shown for both the 45-deg forward- and 45-deg aft-swept wings. For comparison, the duct pressure supplied to the wing slot (and therefore $\dot{m}V_j$) is assumed to be the same as that for the unswept wing at $C_\mu = 0.04$. This results in a higher C_μ on the swept wing due to the reduction in chordwise velocity caused by the sweep. Recall that the definition of C_μ has q in the denominator. Therefore, a 45-deg swept wing with the same compressor setting as the unswept wing would have a blowing level of $C_\mu = 0.08$.

The C_μ values of 0.04 and 0.08 were used as high blowing levels for the unswept and swept wings, respectively. The

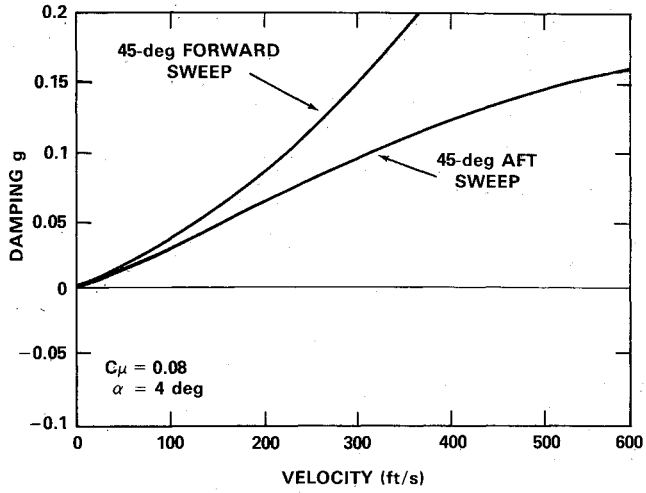

Fig. 9 Effect of wing sweep on CC flutter at high blowing.

Table 3 Results and trends for baseline wing

Parameter	Classical flutter	CC flutter
Mechanism of instability	Coalescence of two modes	Single degree of freedom, due to negative lift slope
Nature of flutter	Usually catastrophic, high speed	Observed limit cycle to date, low speed
Angle of attack	No effect below α-stall angle	Occurs only in narrow range of α
Blowing level (C_μ)	N/A	Higher blowing decreases stability
Reduced torsion stiffness GJ	Destabilizing Lowers divergence speed	No effect
Elastic axis		
Forward:	Stabilizing	No effect
Aft:	Destabilizing	
Increased bending stiffness EI	Slightly stabilizing	Stabilizing
Sweep angle		
Forward:	Causes divergence	Destabilizing
Aft:	Stabilizing	Slightly stabilizing
Unsteady aero, $C(k) = 1.0$	Destabilizing	Destabilizing
C_μ-α stall distribution		
Root:	N/A	Stabilizing
Tip:	N/A	Destabilizing
Blowing distribution		
Root:	N/A	Stabilizing
Tip:	N/A	Destabilizing

results indicate that forward sweep is destabilizing to CC flutter and aft sweep is stabilizing. In spite of the large amount of sweep, coupling between the first bending and torsion modes is very weak. The reason for this is that the frequencies of these two modes start off very well separated for the baseline configuration and no dynamic (mass) bending-torsion coupling is present, since the c.g. coincides with the elastic axis. Frequency trends for both wings are similar to the trends shown in Fig. 5a. Results for the unswept wing are presented in Fig. 6b. If damping were plotted to higher speeds, static divergence would occur first on the aft-swept

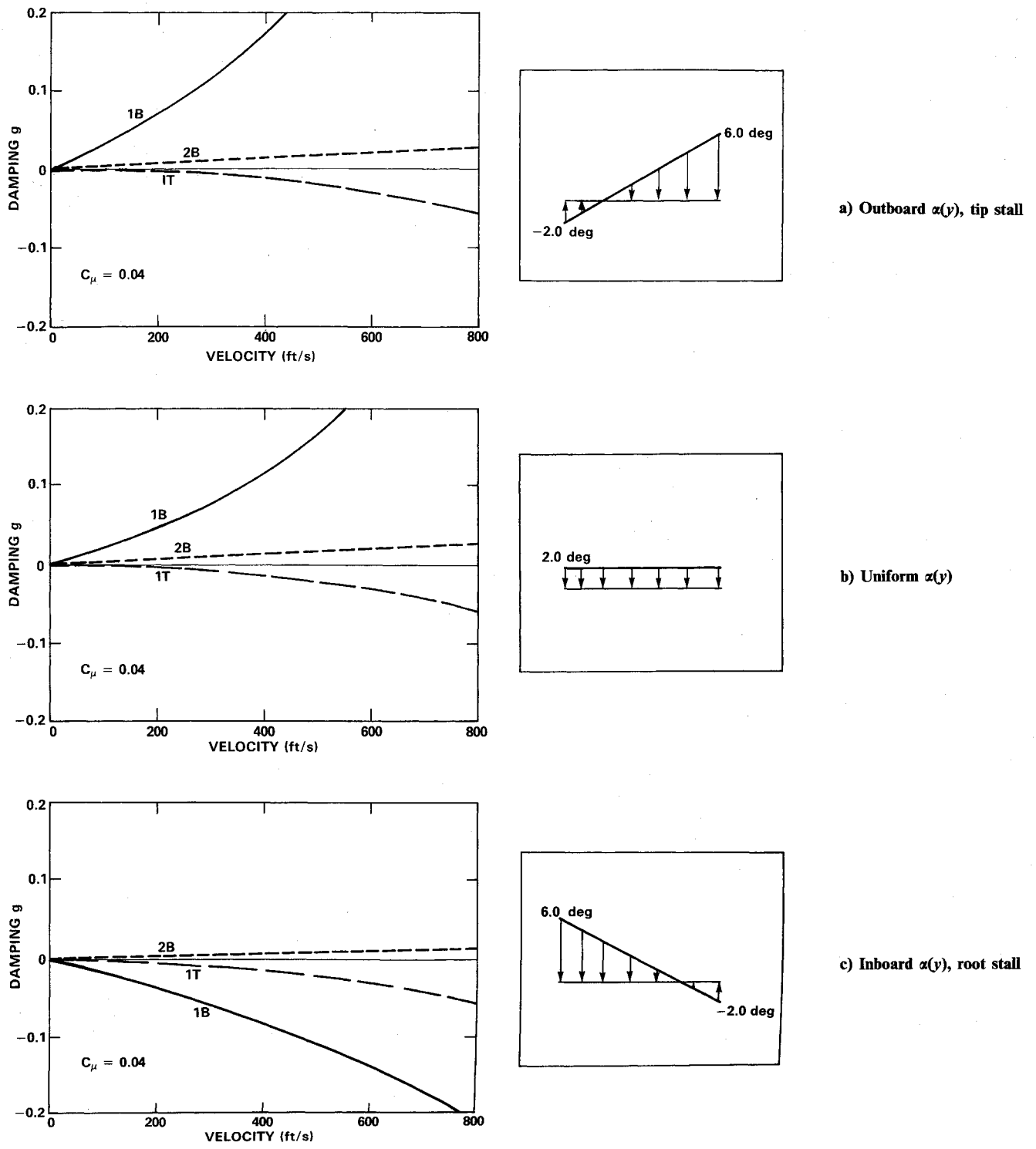

Fig. 10 Effect of spanwise angle-of-attack distribution for an unswept wing at high blowing.

wing (unlike a conventional unblown wing) due to the negative lift curve slope associated with C_μ-α stall.

For the results presented in Figs. 4–9, the steady-state angle-of-attack distribution along the span is constant since the three-dimensional aerodynamic effects are not considered. In order to qualitatively determine the importance of three-dimensional aerodynamic effects, several prescribed spanwise angle-of-attack distributions (pretwist) are examined that represent both inboard and outboard stall conditions. The stability results for three linear twist distributions are shown in Fig. 10. All three wings are set at the same blowing level ($C_\mu = 0.04$) and produce approximately the same amount of lift. At this blowing level, the C_μ-α stall angle of attack is 0 deg. The results indicate that C_μ-α stall at the tip is very detrimental to CC flutter stability. Conversely, a large inboard portion of the wing (more than 60%) can be in a condition of C_μ-α stall, and the wing remains free of flutter. From this example, the importance of including three-dimensional aerodynamic effects is evident if quantitative flutter results are desired.

In a previous study,[4] the distribution of spanwise blowing was used to improve control effectiveness on an aft-swept CC wing. To determine the effect of spanwise blowing distribution on CC flutter, the three linear variations of blowing used in Ref. 3 were examined. For the unswept wing, blowing level varies from $C_\mu = 0.0$ to a maximum value of 0.04; for the

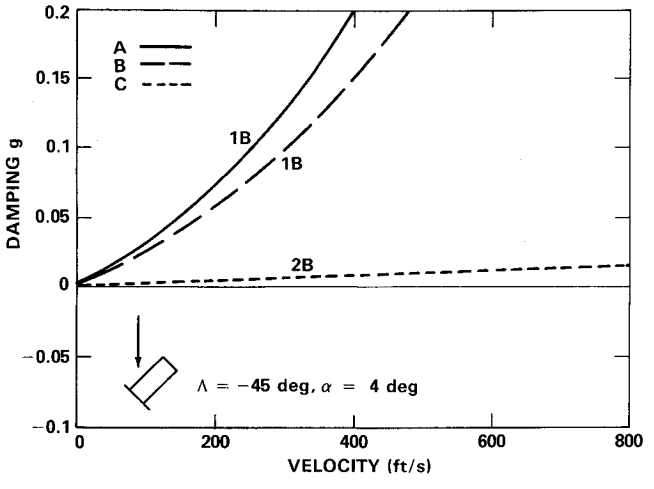

Fig. 11 Damping in least stable mode for 45-deg forward-swept wing.

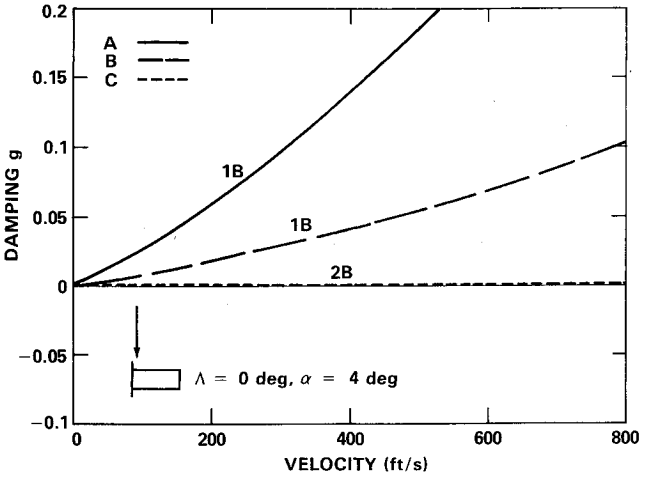

Fig. 12 Damping in least stable mode for unswept wing.

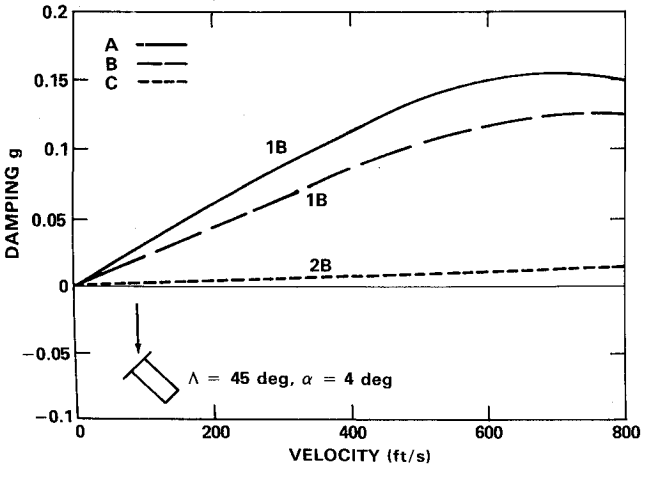

Fig. 13 Damping in least stable mode for 45-deg aft-swept wing.

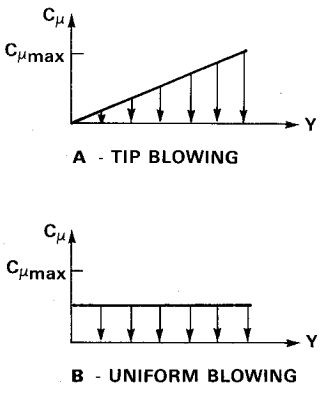

45-deg swept wing, blowing level varies from $C_u = 0.0$ to a maximum value of 0.08.

Results for the 45-deg forward-swept wing, the unswept wing, and the 45-deg aft-swept wing are shown in Figs. 11–13. These figures show damping in the least stable mode for each of the three blowing distributions. In this case, the least stable mode is either the first bending mode ($1B$) or the second bending mode ($2B$), depending on which blowing distribution is used. Regardless of sweep angle, the root blowing distribution is most stabilizing and the tip blowing distribution is most destablizing for CC flutter. In fact, the root-weighted blowing distribution completely stabilizes the first bending mode of the wing from CC flutter. These results illustrate the importance of spanwise blowing distribution as a design parameter for a CC wing.

The linear analysis used in this study can predict only the onset of an instablity. In wind-tunnel tests of CC wings, the CC flutter instability has appeared as a limit cycle oscillation. These experimental observations indicate another characteristic of CC flutter that is fundamentally different from classical flutter. The reason for the limit cycle nature could be that the wing oscillations grow until the α-stall angle is reached and

flow separation occurs. Table 3 summarizes the results and qualitative trends for classical and CC flutter for the baseline wing.

Conclusions

The aeroelastic stability of a high aspect ratio wing with circulation control airfoils has been examined. Two-dimensional static CC airfoil data were used with the modified unsteady aerodynamic strip method to calculate aerodynamic loads. A flutter instability unique to CC wings has been identified and is termed CC flutter. The CC flutter instability occurs at relatively low speed and only at angles of attack between the C_μ-α stall angle and the α-stall angle when sufficient blowing is applied. The mechanism of the CC flutter instability is the negative lift curve slope associated with high blowing levels at angles of attack greater than the C_μ-α stall angle. This instability is a single-degree-of-freedom bending-mode flutter. Outboard C_μ-α stall was shown to aggravate CC flutter more so than root stall. A root-weighted blowing distribution was demonstrated to be an effective means of stabilizing the wing from CC flutter.

References

[1]Englar, R. J. and Applegate, C. A., "Circulation Control—A Bibliography of DTNSRDC Research and Selected Outside References," DTNSRDC Rept. 84-052, AD A146-966, Sept. 1984.

[2]Logan, A. H., "Design and Flight Test of the No Tail Rotor (NOTAR) Aircraft," *38th Annual Forum Proceedings of the American Helicopter Society*, Anaheim, CA, May 1982.

[3]Chopra, I., "Aeroelastic Stability of a Bearingless Circulation Control Rotor in Forward Flight," *Journal of the American Helicopter Society*, Vol. 33, July 1988, pp. 60–67.

[4]Haas, D. J. and Chopra, I., "Aeroelastic Characteristics of Swept Circulation Control Wings," *Journal of Aircraft*, Vol. 25, Oct. 1988, pp. 948–954.

[5]Wilkerson, J. B., "Aeroelastic Characteristics of a Circulation Control Wing," DTNSRDC Rept. 76-0115, AD, Sept. 1976.

[6]Raghavan, V., Pai, S., and Chopra I., "Circulation Control Airfoils in Unsteady Flow," *Journal of the American Helicopter Society*, Vol. 33, Oct. 1988, pp. 28–37.

[7]Yates, E. C., Jr., "Modified-Strip-Analysis Method for Predicting Wing Flutter at Subsonic to Hypersonic Speeds," *Journal of Aircraft*, Vol. 3, Jan–Feb. 1966, pp. 25–29.

[8]Dowell, E. H., Curtiss, H. C., Scanlon, R. H., and Sisto, F., *A Modern Course in Aeroelasticity*, 2nd ed., Sijthoff & Noordhoff, Rockville, MD, 1980, Chap. 3.

[9]Rogers, E. O., Schwartz, A. W., and Abramson, J. S., "Applied Aerodynamics of Circulation Control Airfoils and Rotors," *Vertica*, Vol. 12, No. 1/2, 1988, pp. 69–82.

[10]Wood, N., "Circulation Control Airfoils Past, Present, Future," AIAA Paper 85-0204, Jan. 1985.